Journal of Manufacturing Processes 64 (2021) 1214–1222

Contents lists available at ScienceDirect

Journal of Manufacturing Processes

journal homepage: www.elsevier.com/locate/manpro

Preliminary study of phase-shifting strobo-stereoscopy for cutting tool monitoring

Xiangyu Guo, ChaBum Lee *

J. Mike Walker' 66 Department of Mechanical Engineering, Texas A&M University, 3123 TAMU, College Station, TX, 77843-3123, USA

ARTICLE INFO

Keywords:
Cutting tools
Monitoring
3D imaging
Strobo-stereoscopy
Illumination control
Spindle control

ABSTRACT

Monitoring cutting tool quality in the machining process is essential to the success of part manufacturing. To directly monitor the information of cutting tools under the drilling or milling operations, this paper presents a novel 3D imaging technique to enable direct cutting tool geometry measurement. This method combines stroboscopy and stereoscopy, this strobo-stereoscopy, which synchronizes the stroboscopic illumination system with the spindle control system and enables in-situ reconstructing 3D images of cutting tools. For the phase-locked mode, this technique can lock the image of the cutting tool while in motion. On the other hand, for the phase-shifting mode, all facets around the cutting tool will be scanned by shifting the phase of the light signals while collecting dimensional target information. Experimental studies of phase-locked and phase-shifting modes for monitoring an end mill tool and a wood rolling pin were presented. The directly measured maps and whole 3D images on the target tools verify the capability of the geometry identification of the proposed strobo-stereoscopic imaging technology. Lastly, the potential applications of the proposed technology were discussed.

1. Introduction

Cutting tool wears caused by intensive mechanical stress and high temperature at the tool edge critically affects tool life, manufacturing performance, and products quality [1–5], which in turn depends on the cutting modes (e.g., turning, milling, and drilling) as well as the cutting conditions and cutting fluid [6–8]. With the progress of macro-micro wears, the edge morphology and dimensional accuracy of the cutting tool deteriorate, requiring replacement of the worn cutting tool. While tool replacement is done following a schedule in mass production systems with high cost (25 % of total machining costs), the study suggests that cutting tools are typically utilized only up to 70–80 % of their optimum life [9]. To optimize machine productivity and the quality of products, the cutting tool inspection process is absolutely required in many machining environments.

Common cutting tool measurement and inspection methods based on the monitoring information can be divided into indirect and direct methods. Indirect methods, in which various sensors' signals correlating to tool wear have been extensively applied to the online prediction of tool wear detection [10,11]. Cutting force is one of the popular choices for indirect methods because of its simplicity and fundamental nature of turning operation [12]. Spindle motor and feed motor current, because it correlates with tool cutting forces, are also considered as tool wear health indicators as it is one of the most effective means of monitoring tool wear and adaptive control of machining processes [13]. Other information related to the cutting force like torque, voltage, and speed is also applied to analyze the cutting tool conditions. Another common parameter is acoustic emission (AE) information [14–16]. This method is a more sensitive and accurate alternative than cutting force and can detect micro-scale deformation mechanisms within a relatively 'noisy' machining environment [17]. The indirect methods can be implemented in the on-machine process; however, it is easy to be affected by the environment and cannot offer the direct cutting tool surface quality.

Direct methods where the actual tool wear is measured are more accurate and flexible [18]. Machine vision [19,20] has been pursued for over three decades. A few industries focused on developing tool quality inspection instruments based on machine vision [21]. Scanning electron microscope (SEM), atomic force microscope (AFM), and coordinate measuring machine (CMM) are used to measure cutting tool wear parameters [22–24]. The knife-edge interferometry [25,26] method was also investigated to monitor the edge of cutting tools condition. More advanced measuring techniques using white light interferometry or confocal microscopy can be applied when a nanoscale analysis is necessary [27–30]. While the current practice is for a machine operator

* Corresponding author.
E-mail address: cblee@tamu.edu (C. Lee).

https://doi.org/10.1016/j.jmapro.2021.02.053
Received 20 November 2020; Received in revised form 22 February 2021; Accepted 26 February 2021

to inspect the cutting tool conditions visually, direct measurements are rarely feasible, cost-effective or reliable to perform in real-time due to continuous contact between the tool and the workpiece and the presence of coolant and chips [31–33]. These methods involve a time-consuming process requiring a machine operator to remove the cutting tool from a tool fixture to inspect the cutting tool.

The degradation of product quality due to wear and increasing product cost owing to frequent replacement of tools is the major issue in high-speed machining [34]. Changing cutting tools based on the tool wear condition requires a monitoring system. Lack of such metrology causes the low quality of products and may eventually lead to machine damage with unnecessary expense [35]. While the cost of the sensor (accelerometer, AE, etc.) plays a significant role in implementing the cutting tools monitoring systems, the visual monitoring system (machine vision system) is more flexible and inexpensive and can also be operated and controlled remotely, helping unmanned production systems [18]. Thus, the development of integration of in-process visual metrology in manufacturing processes is becoming increasingly important. García-Ordás et al. [36] applied the image texture analysis method to distinguish the worn-out and non-worn-out tools based on the image characteristic. Pfeifer and Wiegers [37] developed a cutting tool edge wear inspection based on light reflectance and based on this method, Hou et al. [38] implemented the self-matching algorithm for the lower absolute values of errors on the maximum wear width which are less than 0.007 mm. There is few studies on the stereoscopic method, which can offer the possibility to construct the 3D images of the target tool in the whole view.

Inspired by the long-established stroboscope techniques [39], which uses a visual phenomenon caused by aliasing, a series of still samples represent high-speed continuous motion, along with the modern machine vision techniques [19,20], we developed a phase-shifting strobo-stereoscopic cutting tool monitoring method. While the stereoscopic system offers the depth information of the target tools, the stroboscopic technique offers the shifting information of the metrology system. Thus, a 360-degree full-view reconstruction can be achieved for the target sample, which makes the whole-view machine tool monitoring process possible. The proposed technique can be applied to the on-line metrology of drilling and milling tools in the metal cutting industry. The experimental case studies using an end mill tool (ø1/8″) are presented to prove the performance of the proposed cutting tool monitoring technique. Besides, the future work to enable improvement of the proposed strobo-stereoscopy performance was discussed, and an experiment to show the potential to the roll-to-roll manufacturing for pattern recognition on a patterned wood rolling pin was performed.

2. Measurement

In this article, stroboscopy and stereoscopy were combined to in-process measure the 3D images of the cutting tool while in motion. The methodology schematic of the strobo-stereoscopy metrology was presented in Fig. 1. While the stereoscopy algorithm can provide a 3D image at a specific measurement position, the phase-shifting of the strobo-light allows the whole-view reconstruction of the cutting tool while the tool is rotating with a frequency F_0. The encoder signals from the spindle rotation are applied for the stroboscopic light control, so the specific area of the cutting tool can be illuminated by blinking the LED (light-emitting diode) light. The illumination system and camera system can be synchronized with the spindle motion. The measurement operations are automated and digitalized by the LABVIEW and MATLAB software.

2.1. Stroboscopic effect

The stroboscopic instrument is typically applied for the measurement of fast-moving objects. The operation principle is as follows: when synchronizing the light source illumination frequency and the motion of the object, the object appears to be stationary. If minor differences are added to the frequency, the object appears to be slowly moving or rotating. This slow-motion can be working as the source for the phase-shifting; with this phase information, the target can be whole-view 3D reconstructed by 360 degrees. In the experiment setup, the encoder index (Z) from the spindle motion is applied as the trigger for the LED light, as it represents the end of one cycle of a rotary motion. When the proposed technique is operated under the phase-locked mode, no delay information will be implemented to the system. On the contrary, when the system works under the phase-shifting mode, a delay signal related to the spindle working RPM (revolution per minute) and desired stitched map number should be added.

2.2. Stereoscopy imaging system

The stereoscopic technique is embedded with two CCD (charge-coupled device) cameras capturing images located bilaterally symmetrically regarding the target. By applying the triangulation, lens equation, and aberration elimination method. The 3D scene is reconstructed by the location information of the same object points from both the left and right images. Fig. 2 shows the principle of the stereoscopic imaging process.

Camera 1 and 2 with their own coordinate system on the CCD frame and same f, which is the focal length of the lens system, B is the base line

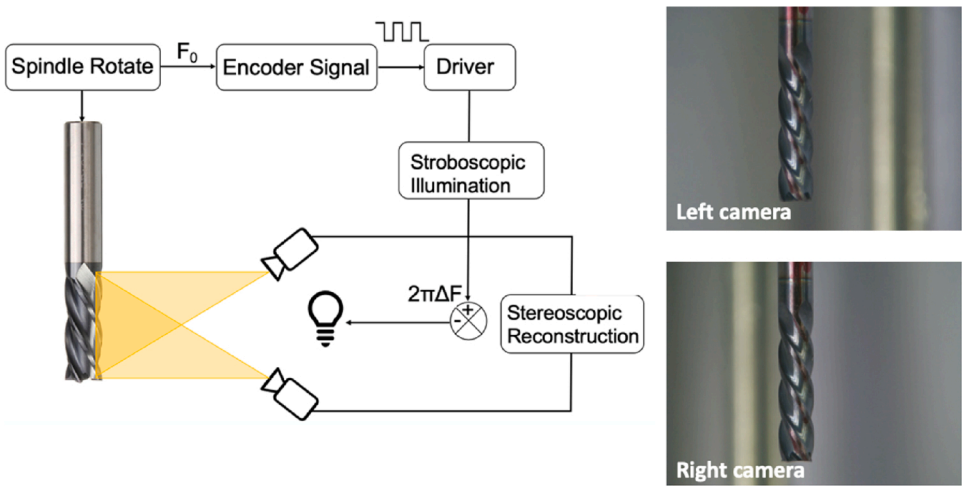

Fig. 1. Methodology schematic of strobo-stereoscopy imaging for drilling/milling tools metrology and inspection.

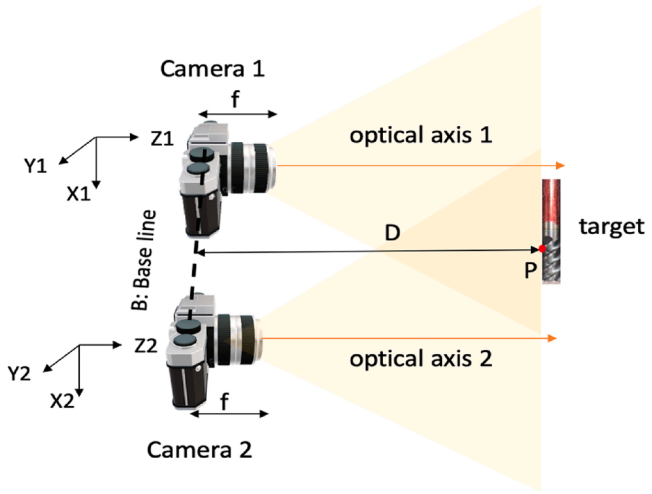

Fig. 2. Stereoscopic system principle.

and D is the measured distance from the point P on the target to the CCD of the camera system.

$$D = f\left(\frac{B}{y_2 - y_1} - 1\right) \tag{1}$$

A stereo camera calibration is performed to determine the intrinsic and extrinsic camera parameters or the projection matrix coefficients of the system [40]. These parameters transfer the scene points in 3D space to their corresponding image points, thus the measured depth can be recovered. In this study, calibration was performed with the same camera systems for the target sample measurement.

The Stereo Camera Calibrator app in MATLAB was applied to the calibration process, note that the mathematical algorithm for computing camera parameters used in solving the camera calibration problem is beyond the scope of this paper. 20 images of calibration checkboard pattern at different orientations related to the cameras were taken by the stereoscope system. Fig. 3 shows 3 pairs of calibration checkboard patterns for the parameter calibrations.

2.3. D surface reconstruction and phase-locked phase-shifting algorithm

A 3D printed reference array with 4 mm diameter and 4 mm height cylinders on was applied as the reference target to prove the 3D surface reconstruction process. The target is shown in Fig. 4. The reconstruction process on one of the cylinders is in Fig. 5.

The 3D reconstruction is based on the stereoscopic method, the working principle is shown in Fig. 5(a). After gathering the depth map, tip/tilt (this information could be observed in Fig. 5(c) depth map and noise information would exist in the raw image. The system error removal process was applied to remove the unbalanced information from the reconstruction depth map Fig. 5(d). The gaussian filter is applied to decrease the noise level and smooth the surface map. Once the surface map was achieved, the validation was performed.

Linear measurement results are extracted from Fig. 5(d), which are presented below, where the average value of the height from Fig. 6(a) on the proposed method is 4.08 mm. Because the part was 3D printed by fused deposition modeling, the printing patterns were also observed in Fig. 6(b). The target linear-scanned results (blue) are compared with the dial-gauge (resolution of 0.001 mm) testing result (orange), as shown in Fig. 6(b) as well. Fixed with a motorized linear axis, set the initial dial-gauge value to be 0 when it is at the edge of the target structure, the data was read out every 0.5 mm along the same-measured direction by the proposed method(Fig. 6(d)). The dial gauge indicated the height is approximately 4.15 mm, and the height variation was observed in Fig. 6 (c). The probe-based measuring tools are typically limited to accurately

Fig. 4. 3D Printed reference array.

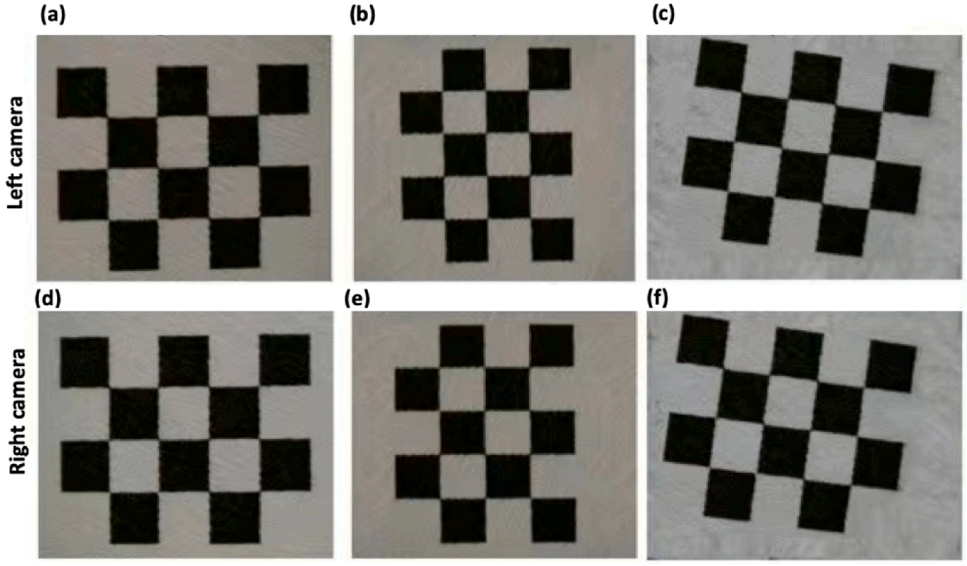

Fig. 3. Examples of checkboard pattern stereo images taken by the stereoscopic system, where pair images 1 are (a), (d), pair images 2 are (b), (e), and pair images 3 are (c),(f).

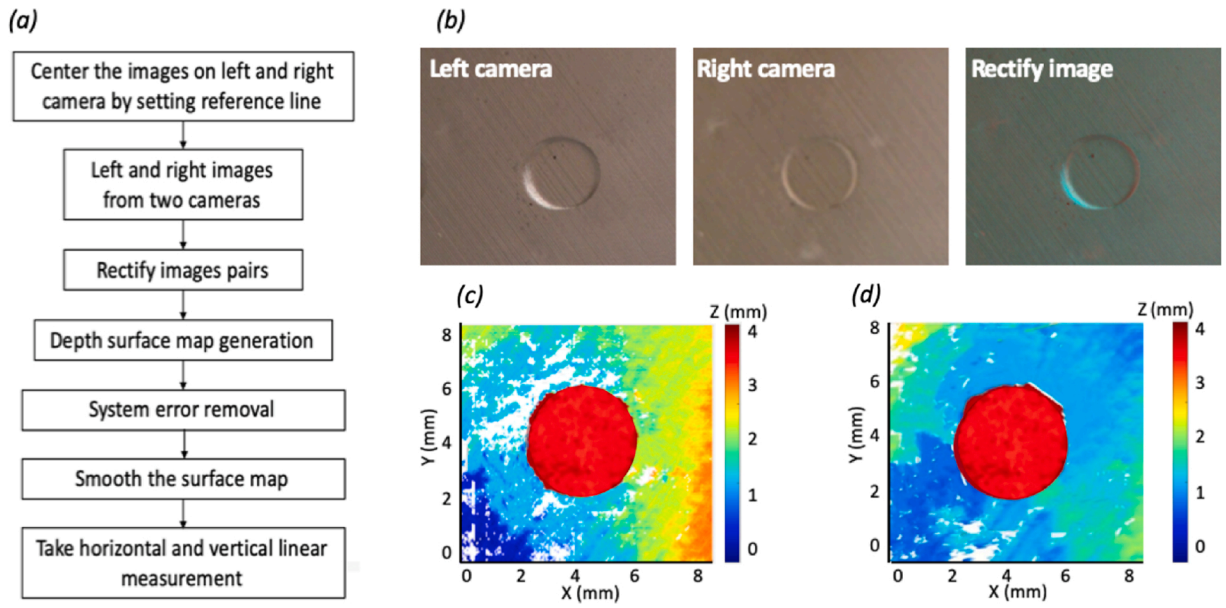

Fig. 5. Stereoscopic reconstruction process (a), example on stereoscopic reconstruction process (b), depth map(c) and system error removed and filtered map (d).

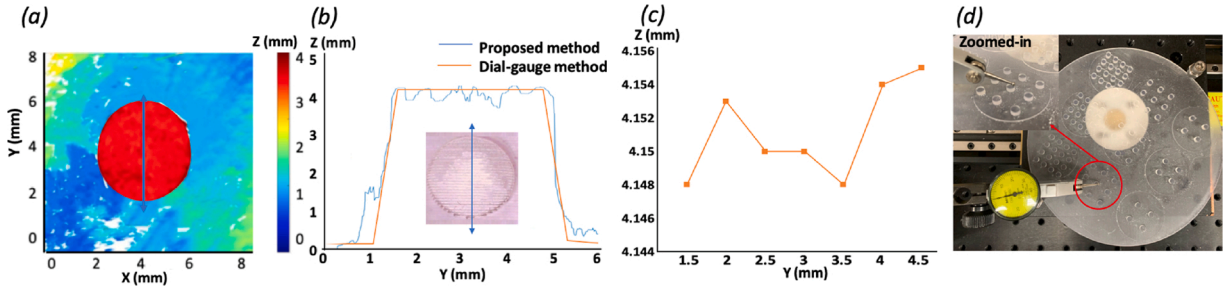

Fig. 6. 3D printed part surface map (a), the linear extract measurement in the blue arrow line location (b), dial-gauge measured height variation (c), and dial-gauge measurement set-up (d) (For interpretation of the references to colour in this figure legend, the reader is referred to the web version of this article).

measure the grooves and ridges of the structures smaller than the probe size, but are commonly used to measure the height and the structures. The height discrepancy of two measurement methods showed only 1.7 %.

The phase-locked and phase-shifting algorithm synchronizes the rotational speed RPM (revolution per minute) with the light blinking frequency and shifts the phase of the light signal from 0 to 360 degree. The flow chart of the strobo-light system for the phase shifting process was presented in Fig. 7. This phase-shifting scan method by stroboscopic control algorithm was programmed in the LabVIEW environment.

The rising edge of the Encoder index (Z) signal is used as the signal that the whole cycle of rotation is finished. This signal is related to the rotational speed (RPM), and F is the desired LED blink frequency in Hz. When F is equal to the spindle rotary frequency, both CCDs gather pictures at the single location of the cutting tool. This is also called as the phase-locked mode. When F is different from the spindle rotary frequency, which means we introduce the delayed time T into the system, a sequence of images was gathered under the phase-shifting process for a whole-view 3D reconstruction, this is called as the phase-shifting mode.

First, the desired number of images per cycle N is set N. The parametric relationship can be expressed as:

$$N = \frac{RPM}{RPM - 60F} \tag{2}$$

$$\frac{1}{F} + T = i\frac{60}{RPM} \tag{3}$$

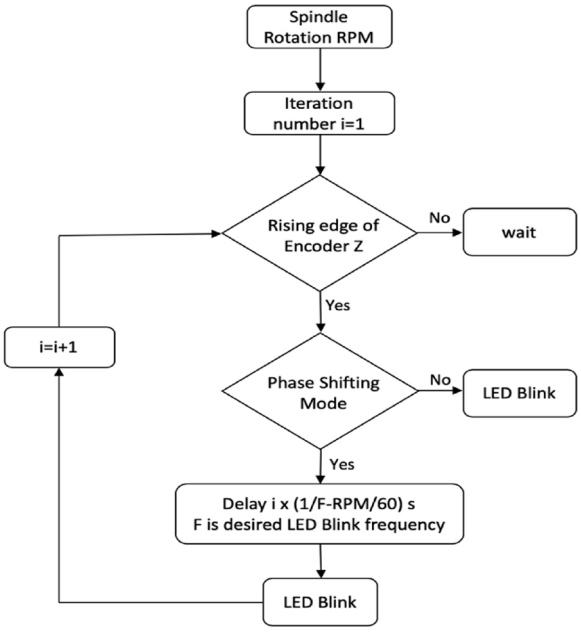

Fig. 7. Flow chart of stroboscopic motion and light control algorithms. i is a positive integer.

From above, the delayed time information t can be calculated as:

$$t = i\frac{60}{RPM} - \frac{60}{RPM - \frac{N}{RPM}} \quad (4)$$

To gather a whole-view 3D surface map, after the phase-shifting process, a stitching algorithm for the depth map reconstruction is required. The full view 3D surface building process was illustrated to explain the depth map reconstruction process as seen in Fig. 8.

3. Experiments

In the proposed system, to minimize the rotational motion error-induced effect, the aerostatic spindle (rotational error < 0.1 μm) with 2048 steps per cycle (encoder signal) was applied, and working under the velocity control mode to secure the motion accuracy and rotational speed. As shown in Fig. 9(a), two CCDs (30 frames per second) with the lenses (field of view: 18 × 24 mm) were installed on two linear rails (x- and z-direction) with rotary stages to capture the raw picture of a cutting tool bit for further 3D reconstruction. Cross lasers on top of each CCD camera were added to guarantee both cameras focus at the exact location of the measurement target. An end mill tool (ø 1/8″) was used as the experimental target as seen in Fig. 9(b).

4. Results

4.1. Phase-locked mode

The developed strobo-stereoscopy measured the cutting tool geometry under 90, 360 RPM. The surface reconstruction maps along with the center vertical linear scanning results were shown in Fig. 10. In Fig. 10 (c), a 1 mm interval was added to present the results clearly. The similar pattern on the center linear scan can be observed.

For each working condition, 5 raw images were captured, the averaged information from the raw images was used to reconstruct the surface map. The construction process was shown in the previous section. These results provided the ability to measure the surface roughness on the edge and flute. For reference, the white areas on the color maps were induced by the void areas (no reflective areas) and the surfaces with high slope. Most microscopic camera systems have limited performance on the collection of stray light.

Vertical linear measurements were applied on the surface map to validate the surface map reconstruction repeatability. The average values and the deviation values of the detected depth of groves (D) and detected length of groves (H) under each working RPM were shown in Table 1.

We also measured the H and D value by digital caliper, which is 2.91 mm and 0.87 mm correspondingly. These results provide the ability to track the tool surface geometry characteristics. The deviation here indicates the difference of H and D along each black, red and blue line. The deviation resulted from the cutting tool geometry, although a few micrometer-scale deviations due to CCD camera pixel size could be involved. From the results, it is obvious that the deviation value remains the same for both 90 and 360 RPM condition, which represents the stable performance of the proposed technique. However, the different average value exits, and this comes from the quality of the "frozen image" under different working RPM.

4.2. Phase-shifting mode

From the phase-locked mode results, when working RPM was 90, the surface reconstruction map showed the most complete results among other tests. Thus, the cutting tool was rotated under 90 RPM for the phase-shifting mode experiment, and the desired number of images per cycle was set to be 18 (20-degree imaging interval). A series of screenshots of the phase shifting 'frozen moment' is shown in Fig. 11.

The center surface reconstruction is based on the stereoscopic algorithm. Before the depth map is recovered, pre-process for target centering, distortion removal, and brightness adjustment need to be done. Gaussian filter is applied to remove system noise. For the neighbor surfaces stitching process, SIFT (scale-invariant feature transform) [41] was used to determine the similar characteristics first, as they provided reference information. After the stitched panorama surface was generated, a whole surface phase unwrapping process was applied to remove the stitching errors. Fig. 12 shows a stitched geometry expanded surface map and a vertical wave-fall map based on the phase-shifting process.

The preliminary study experiment was performed on an end mill tool (ø1/8″), two working modes: phase-locked and phase-shifting modes were simultaneously operated. The phase-locked mode process showed the possibility of reconstructing the surface geometric information, such as surface roughness and shape, and tracking the surface characteristics, such as the grove depth and length. The phase-shifting mode showed the whole-view surface map reconstruction ability (Fig. 13).

5. Future development

For further development on this technique, in addition to CCD with high frame rates, the laser scanning process for the structured light including spectroscopic approaches scan will be added to the system and will also be synchronized with spindle motion and illumination system, which can help collect tool edge conditions and dynamic performances. This combination of strobo-stereoscopy and laser scanning can improve the 3D image quality toward in-process characterization and identification of cutting tool dynamic behavior and cutting tool conditions.

Based on the geometry information reconstruction of the target end-mill tool, another potential of the proposed technique is the pattern recognition and construction for the roll-to-roll manufacturing industry.

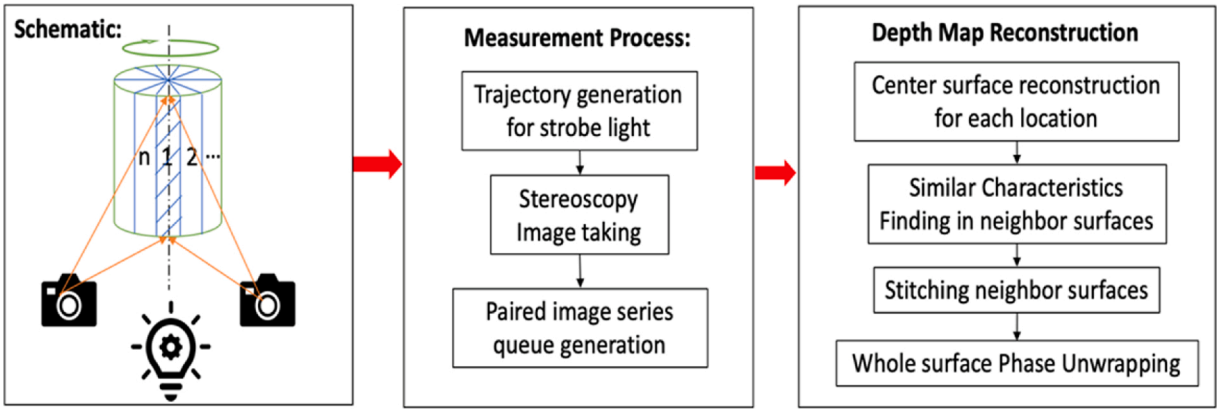

Fig. 8. Whole view 3D surface building process.

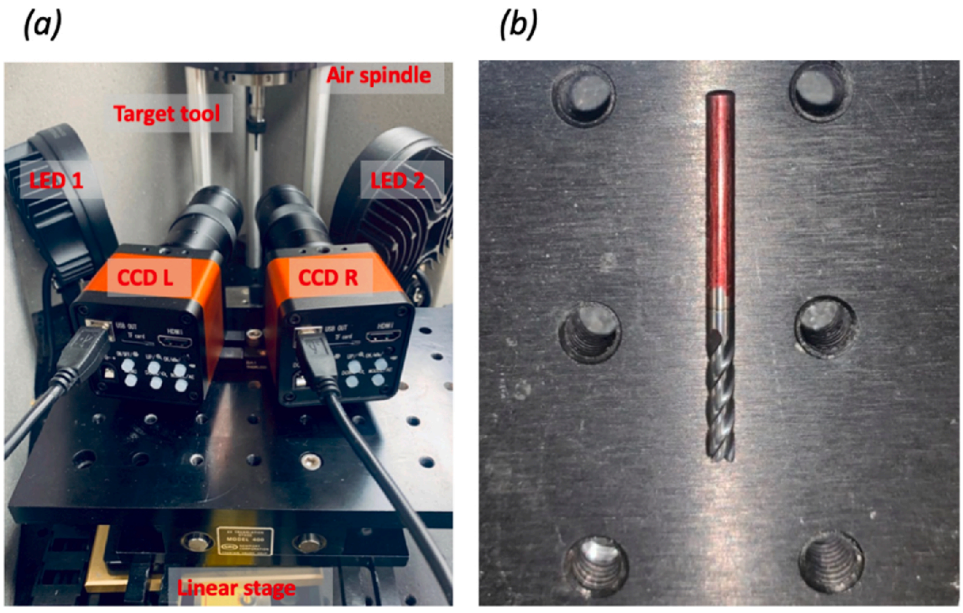

Fig. 9. Experiment set-up of the proposed method (a) and experiment target end mill tool sample (b).

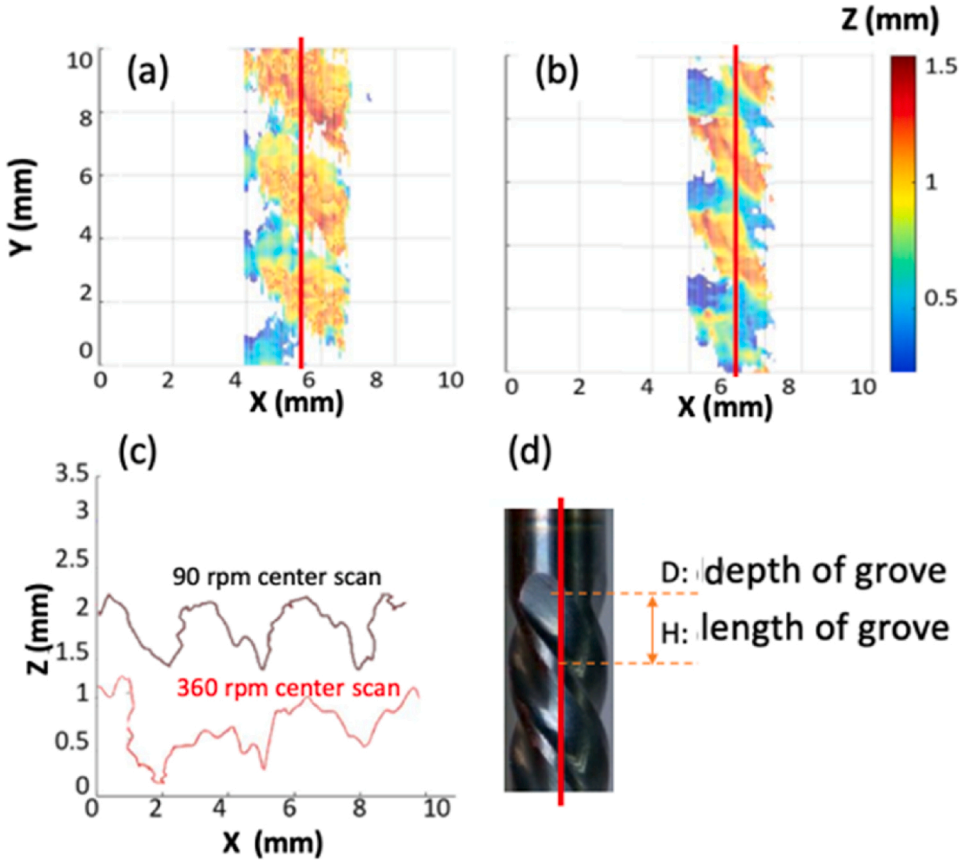

Fig. 10. End mill tool phase-locked surface map at 90 RPM (a) and 360 RPM (b), vertical center linear measurement (c), as well as the corresponded target sample (d).

Here, a demonstration was performed on a dinosaurs-patterned wood rolling pin (ø 76 mm) with 30 RPM, together 18 images were taken for the whole view reconstruction. A series of screenshots of the phase shifting 'frozen moment' is shown in Fig. 14.

Under the same method, Fig. 15(a) showed a stitched geometry of the expanded surface map. Based on the target diameter and the calculated depth information from Fig. 15(a), (b) showed a reconstructed 3D rolling pin map, and Fig. 15(c) represented the top view of the 3D rolling pin map.

As a result, the proposed methods have potentials to offer more detailed and less noise information on the low-speed measurement and can clearly perform the pattern recognition and reconstruction process.

Table 1
Vertical linear measurement results under different working RPM.

Rotation speed	H (mm)		D (mm)	
	Average	Deviation	Average	Deviation
90 RPM	3.03	0.14	0.67	0.08
360 RPM	2.84	0.14	0.83	0.08

Further study on image processing to remove data outliers will improve the image quality.

6. Conclusion

The principle of the phase-shifting strobo-stereoscopic 3D imaging process was first introduced and was preliminarily validated. The measurement system was developed, and the 3D reconstruction algorithms and phase-locked and -shifting algorithms were newly created. The spindle motion was successfully synchronized with strobo-light signals. The preliminary study results showed that the proposed strobo-stereoscopy could in-process measure the cutting tool geometry and reconstruct 3D images in the 360-degree whole-view that have the potential to monitor the tool conditions. The proposed measurement method could be utilized for on-machine measurement in various manufacturing processes. The system performance can be significantly improved by using high-speed cameras with high frame rate and the light illumination system, and this measurement method combined with advanced image processing techniques can achieve less noise and more detailed surface reconstruction, which is able to perform the pattern recognition and reconstruction of various objects in 3D. For the future work, the proposed 3D imaging technology will be further improved by combining strobo-stereoscopy and spectroscopy that can measure not only the 3D shapes but also 3D spectral properties of the rotating target objects. This advanced measurement method will enable to in-process monitor the conditions and status of the target object and the whole system's dynamics.

Authorship

- All authors have participated in (a) conception and design, or analysis and interpretation of the data; (b) drafting the article or revising it critically for important intellectual content; and (c) approval of the final version.
- This manuscript has not been submitted to, nor is under review at, another journal or other publishing venue.
- The authors have no affiliation with any organization with a direct or indirect financial interest in the subject matter discussed in the manuscript

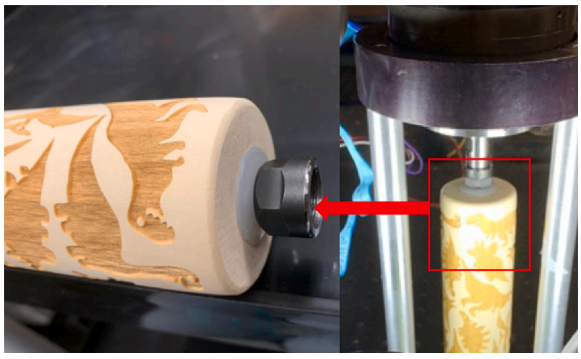

Fig. 13. Dinosaurs-patterned wood rolling pin.

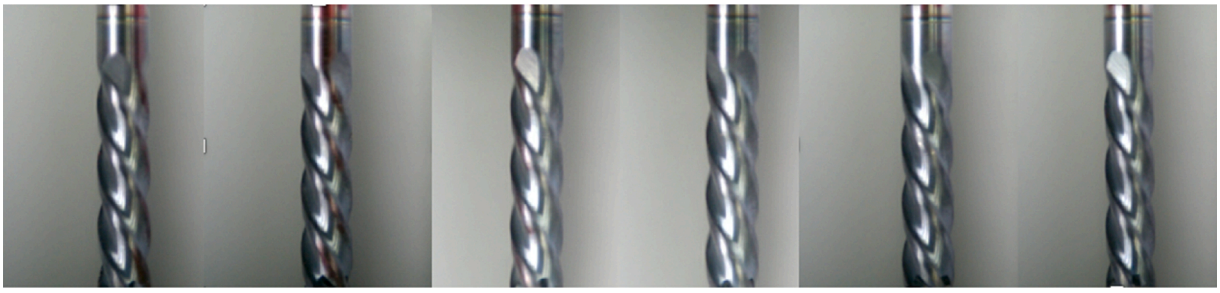

Fig. 11. End mill tool phase-shifting raw image from location 1~6.

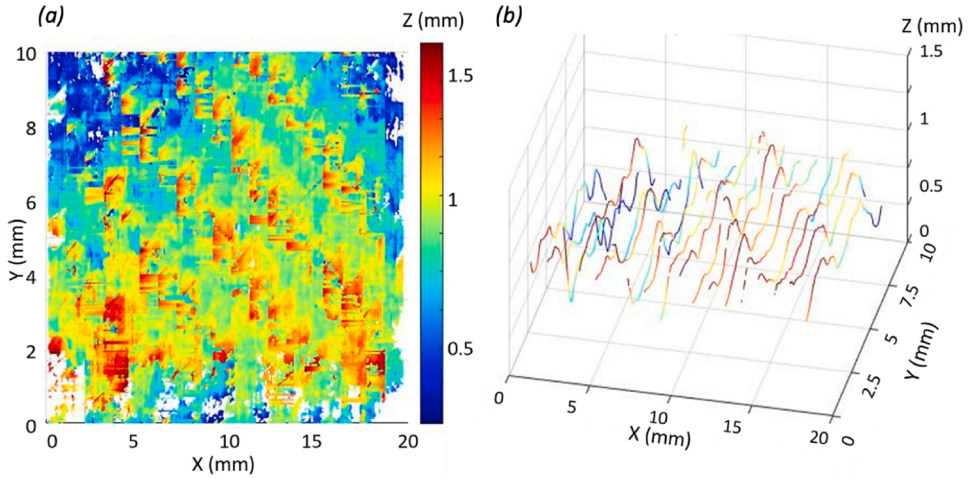

Fig. 12. End mill tool phase-shifting geometry expanded panorama surface map (a) and the vertical wave-fall map (b).

Fig. 14. End mill tool phase-shifting raw image from location 1~5.

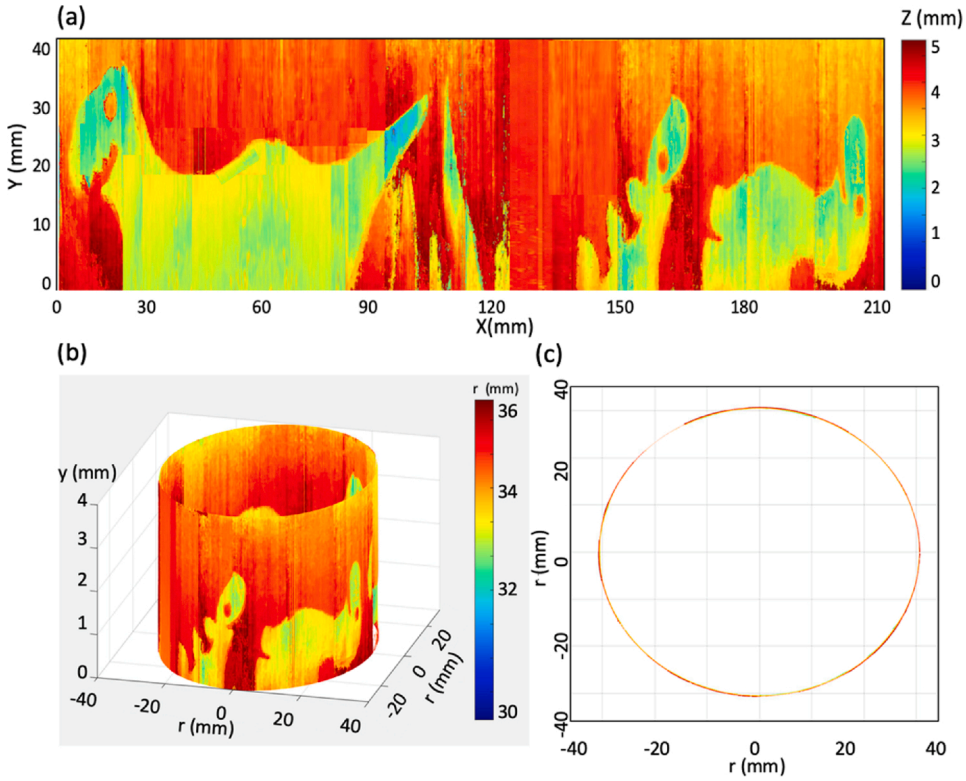

Fig. 15. Dinosaurs-patterned rolling pin whole view reconstruction results, stitched geometry expanded surface map (a), the reconstructed 3D rolling pin map(b) and the top view map (c).

Declaration of Competing Interest

The authors report no declarations of interest.

Acknowledgements

The research was supported by the National Science Foundation (Award Number: CMMI 1902697) through the Texas A&M University.

References

[1] Guo X, Lee C. Phase- shifting 3D imaging of rotating Milling/drilling tools. In: Proceeding of American Society for Precision Engineering Annual Meeting; 2020.
[2] Knight Winston A, Boothroyd Geoffrey. Fundamentals of Metal Machining and Machine Tools. CRC Press; 2019.
[3] Grzesik Wit. Advanced Machining Processes of Metallic Materials: Theory, Modelling and Applications. Elsevier; 2008.
[4] Sheikh-Ahmad Jamal Y. Machining of Polymer Composites. Springer; 2009. 387355391.
[5] Taylor Frederick Winslow. On the art of cutting metals. In: An Address Made at the Opening of the Annual Meeting in New York; 1907.
[6] Hwang Yeon, Kuriyagawa Tsunemoto, Sun-Kyu Lee. Wheel curve generation error of aspheric microgrinding in parallel grinding method. Int J Mach Tools Manuf 2006;46(15):1929–33.
[7] Lee Sun-Kyu, Miyamoto Yuji, Kuriyagawa Tsunemoto, Syoji Katsuo. "Minimization of hydrodynamic pressure effect on the ultraprecision mirror grinding. Int J Precis Eng Manuf 2005;6(1):59–64.
[8] Lee Sun-Kyu, Miyamoto Yuji, Kuriyagawa Tsunemoto, Syoji Katsuo. Effects of minimizing hydrodynamic pressure in ultra-precision mirror grinding. Int J Mach Tools Manuf 2004;44(10):1031–6.
[9] Ghosh Sourath, Naskar Sukanta Kumar, Mandal Nirmal Kumar. Estimation of residual life of a cutting tool used in a machining process. In: 4th International Conference on Engineering, Applied Sciences and Technology; 2018.
[10] Dan Li, Mathew Joseph. Tool wear and failure monitoring techniques for turning—a review. Int J Mach Tools Manuf 1990;30(4):579–98.
[11] Jantunen Erkki. A summary of methods applied to tool condition monitoring in drilling. Int J Mach Tools Manuf 2002;42(9):997–1010.
[12] Rehorn Adam G, Jiang Jin, Orban Peter E. State-of-the-art methods and results in tool condition monitoring: a review. Int J Adv Manuf Technol 2005;26(7–8): 693–710.
[13] Mannan MA, Broms S, Lindström Bo. Monitoring and adaptive control of cutting process by means of motor power and current measurements. CIRP Annals 1989;38 (1):347–50.
[14] Marinescu Iulian, Axinte Dragos A. A critical analysis of effectiveness of acoustic emission signals to detect tool and workpiece malfunctions in milling operations. Int J Mach Tools Manuf 2008;48(10):1148–60.
[15] Chen Hongjiang. Investigation of the methods for tool wear on-line monitoring during the cutting process. International Conference on Computer and Computing Technologies in Agriculture 2010.
[16] Uekita Masahiro, Takaya Yasuhiro. Tool condition monitoring for form milling of large parts by combining spindle motor current and acoustic emission signals. Int J Adv Manuf Technol 2017;89(1–4):65–75.
[17] Lee Dae-Eun, Hwang Inkil, Valente CarlosMO, Oliveira JFG, Dornfeld David A. Precision manufacturing process monitoring with acoustic emission. Condition Monitoring and Control for Intelligent Manufacturing. Springer; 2006. p. 33–54.
[18] Dutta S, Pal SK, Mukhopadhyay S, Sen R. Application of digital image processing in tool condition monitoring: a review. CIRP J Manuf Sci Technol 2013;6(3):212–32.

[19] Szydłowski Michał, Powałka Bartosz, Matuszak Marcin, Kochmański Paweł. Machine vision micro-milling tool wear inspection by image reconstruction and light reflectance. Precis Eng 2016;44:236–44.
[20] Zhang Chen, Zhang Jilin. On-line tool wear measurement for ball-end milling cutter based on machine vision. Comput Ind 2013;64(6):708–19.
[21] Alicona, "Reliable tool quality control using optical 3D measurement technology", OSG Measurement Report.
[22] Gao Wei. Precision Nanometrology: Sensors and Measuring Systems for Nanomanufacturing. Springer Science & Business Media; 2010.
[23] Waters TFrederick. Fundamentals of Manufacturing for Engineers. CRC Press; 2017.
[24] Zhang Chen. Tool wear measurement of ball-end cutter based on shape mapping. Adv Mat Res 2011.
[25] Jeon Seongkyul, Stepanick Christopher K, Zolfaghari Abolfazl A, ChaBum Lee. Knife-edge interferometry for cutting tool wear monitoring. Precis Eng 2017;50:354–60.
[26] Jeon Seongkyul, Zolfaghari Abolfazl, ChaBum Lee. Dicing wheel wear monitoring technique utilizing edge diffraction effect. Measurement 2018;121:139–43.
[27] Jin Jonghan, Kim Young-Jin, Kim Yunseok, Seung-Woo Kim. Absolute distance measurements using the optical comb of a femtosecond pulse laser. Int J Precis Eng Manuf Technol 2007;8(4):22–6.
[28] Debnath Sanjit Kumar, You Joonho, Seung-Woo Kim. Determination of film thickness and surface profile using reflectometry and spectrally resolved phase shifting interferometry. Int J Precis Eng Manuf 2009;10(5):5–10.
[29] Lee Cha Bum, Kang Jin-Ho, Joo Jae-Young, Sun-Kyu Lee. Phase locked loop based topography measurement of ultraprecision machined surface using the ball lensed and tapered fiber. OFS2012 22nd International Conference on Optical Fiber Sensors 2012.
[30] Kang Jin-Ho, Lee Cha Bum, Joo Jae-Young, Sun-Kyu Lee. Phase-locked loop based on machine surface topography measurement using lensed fibers. Appl Opt 2011;50(4):460–7.
[31] Nouri Mehdi, Fussell Barry K, Ziniti Beth L, Linder Ernst. Real-time tool wear monitoring in milling using a cutting condition independent method. Int J Mach Tools Manuf 2015;89:1–13.
[32] He David, Li Ruoyu, Bechhoefer Eric. Stochastic modeling of damage physics for mechanical component prognostics using condition indicators. International Design Engineering Technical Conferences and Computers and Information in Engineering Conference 2009.
[33] Bhattacharyya P, Sengupta D, Mukhopadhyay S. Cutting force-based real-time estimation of tool wear in face milling using a combination of signal processing techniques. Mech Syst Signal Process 2007;21(6):2665–83.
[34] Mohanraj T, Shankar S, Rajasekar R, Sakthivel NR, Pramanik Alokesh. Tool condition monitoring techniques in milling process—a review. J Mater Res Technol 2020;9(1):1032–42.
[35] Snr Dimla EDimla. Sensor signals for tool-wear monitoring in metal cutting operations—a review of methods. Int J Mach Tools Manuf 2000;40(8):1073–98.
[36] García M, Alegre E, Rodríguez R, Castro V. Tool wear monitoring using an online, automatic and low cost system based on local texture. Mech Syst Signal Process 2018;112:98–112.
[37] Pfeifer T, Wiegers R. Reliable tool wear monitoring by optimized image and illumination control in machine vision. Measurement 2000;28(3):209–18.
[38] Hou Q, Sun J, Huang PA. Novel algorithm for tool wear online inspection based on machine vision. Int J Adv Manuf Technol 2019;101:2415–23.
[39] Zinin EI. Stroboscopic method of electro-optical picosecond-resolution chronography and its application in synchrotron radiation experiments. Nucl Instrum Methods Phys Res 1983;208(1–3):439–41.
[40] Faugeras Olivier. Three-Dimensional Computer Vision: A Geometric Viewpoint. MIT press; 1993.
[41] Lu Z, Réhman Su, Khan MSL, Li H. Anaglyph 3D stereoscopic visualization of 2D video based on fundamental matrix. In: International Conference on Virtual Reality and Visualization; 2013. p. 305–8.